Efficiency enhancement of multi-relay wireless power transfer system using switched compensation capacitors

Xinyu Hou[1*], Meiqi Yang[1], Yong Shi[1], Zhongming Yu[2] and Zixuan Zhao[1]

[1] *Shaanxi University of Science & Technology, School of Electrical and Control Engineering, Xian 710021, China*
[2] *Kunming University of Science and Technology, Faculty of Electric Power Engineering, Kunming 650500, China*
* Corresponding author, E-mail: houxinyu@sust.edu.cn

Abstract

Multi-relay wireless power transfer (WPT) systems are increasingly used in power supply applications for high-voltage transmission line monitoring due to their extended transmission range. However, such systems face challenges from frequency-splitting phenomena, where multiple resonant frequencies render fixed compensation networks ineffective. To address this, a switchable compensation capacitor matrix is proposed to replace the resonant capacitor in LCC-S compensation networks. First, the transmission efficiency and constant current/voltage output characteristics of a four-coil multi-relay WPT system with LCC-S compensation are investigated. Then, the transmitter-side resonant capacitor is replaced with a switchable capacitor matrix to achieve stable output performance. Experimental results demonstrate that the modified system can dynamically adjust compensation capacitance according to input frequency variations, effectively matching the required resonant conditions. The feasibility of the proposed method is verified through a four-coil multi-relay WPT system prototype implementation, showing improved frequency adaptability while maintaining system efficiency.

Introduction

With technological advancements, traditional power transmission faces security challenges and inherent limitations. Wireless power transfer (WPT), known for its safety, reliability, and low maintenance, is increasingly used in electric vehicles[1], biomedicine[2], and other specialized applications.

Due to environmental and climatic factors[3,4], wired power supply faces significant limitations in online monitoring equipment for high voltage transmission line[5]. As a result, WPT is increasingly adopted as an alternative power solution. Furthermore, since conventional two-coil systems can no longer meet the demands for long-distance transmission, researchers have begun to explore and utilize multi-relay WPT systems.

However, in the process of wireless power transfer, various methods have been explored to improve transmission efficiency, with optimizing the compensation network being the preferred solution. For multi-relay WPT systems, the frequency-splitting phenomenon results in multiple resonant frequencies, rendering fixed compensation networks inadequate to address frequency splitting and its negative effects[6,7]. To solve this problem, a switch-controlled capacitor (SCC)[8] has been employed to dynamically reconfigure the compensation network, enabling real-time switching of resonant frequencies to enhance system performance, such as transmission power and efficiency.

A hybrid control strategy integrating phase shift modulation (PSM) with a switch-controlled capacitor (SCC) is proposed[9]. An additional SCC component is integrated into the LCC-S compensation network, and its operation is regulated through feedback. This approach reduces the losses in the primary coil under light-load conditions and enhances the system's transmission efficiency. A reactance elimination method based on an impedance buffer is proposed[10]. This method achieves full-range zero-phase angle (ZPA) operation by connecting a synchronous impedance buffer in series with the CLC compensation network, thereby eliminating

reactance. A method incorporating a controllable switched capacitor (SCC) into the compensation network is proposed[11], adjusting the total output power and input impedance by regulating the inverter's duty cycle and transmitter-side compensation capacitance. The studies show that optimizing the compensation network improves transmission efficiency and enables constant current (CC) and constant voltage (CV) output. A zero-voltage switching (ZVS) controller design method for WPT systems is proposed[12], using a feedback controller and a five-stage variable capacitor. This ensures the ZVS angle remains at the reference angle during load changes, achieving reliable control. However, the SCC approach necessitates intricate parameter identification as a prerequisite and depends on communication support, resulting in higher costs, greater system complexity, and reduced robustness. Moreover, its continuous adjustability introduces substantial energy losses. The method of synchronizing the buffer and inverter sections increases system complexity and cost due to the required coordination between two sets of drive frequencies.

The study analyzes the transmission characteristics of a four-relay multi-coil wireless power transfer (MC-WPT) system in series-series (S-S) and series-parallel (S-P) topologies and proposes a global tracking method to achieve optimal transmission efficiency under variable load conditions by switching between S-S and S-P topologies[13]. This study proposes an improved design method for both the coupling mechanism and compensation capacitors in multi-relay WPT systems based on segmented compensation. This approach effectively addresses the issue of sudden voltage spikes occurring in partial coils and at resonant capacitor terminals when the system operates at constant-voltage frequency[14]. Multi-relay coil WPT systems can significantly extend transmission distance and improve operational flexibility, but they also introduce notable technical challenges. These systems are prone to frequency-splitting phenomena, resulting in multiple resonant peaks that lead to unstable power transfer efficiency. A key unresolved issue is how to

rapidly switch compensation capacitors to enable the system to achieve maximum transmission efficiency quickly.

To address these challenges, a multi-stage switched capacitor matrix method is proposed. This switched capacitor matrix, functioning as a configurable compensation capacitor, is particularly suitable for high-frequency applications. It employs relay-controlled discrete signals to switch different branches, thereby reducing losses caused by continuous signal operation. First, a mathematical model of the four-coil multi-relay LCC-S compensation network WPT system is developed, analyzing its transmission efficiency as well as constant current (CC) and constant voltage (CV) characteristics. Next, transmission efficiency curves are derived for different loads and resonant frequencies. The resonant capacitance of the transmitter is then adjusted to achieve CC or CV output under varying input frequencies and loads, ensuring high efficiency. Finally, an experimental platform is built to verify the effectiveness of the proposed method.

Modeling of multi-relay LCC-S system

Figure 1 illustrates the circuit topology of the LCC-S type multi-relay WPT system. Here, U is the DC input power supply, $\dot{U}_s$ is the inverted output voltage, S_1, S_2, S_3, and S_4 form the inverter circuit, L_{P1} is the resonant inductor, C_{P1}, C_P, C_1, C_2, and C_S are the resonant capacitors, The C_{P1} compensation capacitor matrix, whose structure is illustrated in Fig. 1, L_P is the self-inductance of the transmitting coil, L_1 and L_2 are the self-inductances of the relay coils, L_S is the self-inductance of the receiving coil, M_{ij} ($i, j \in$ N*) represents the mutual inductance between coil i and coil j, $\dot{I}_S$ is the inverter output current, $\dot{I}_P$ is the current vector of the transmitting coil, $\dot{I}_1$ and $\dot{I}_2$ are the current vectors of the relay coils, $\dot{I}_3$ is the current vector of the receiving coil, D_1, D_2, D_3, and D_4 form the rectifier circuit, C_L is the filter capacitor, R_L is the load resistance, and r_P, r_1, r_2, and r_3 are the equivalent internal resistances of coils L_P, L_1, L_2, and L_S, respectively.

The equivalent circuit diagram of the LCC-S compensation network multi-relay MC-WPT system is shown below. The transmitter-side compensation network consists of L_{P1}, C_{P1}, and C_P, while the receiver-side compensation network includes only C_S. $\dot{I}_S$ and $\dot{I}_3$ repre-

sent the input and output currents, respectively. The DC voltage source U and the inverter in Fig. 2 are collectively equivalent to the AC voltage source $\dot{U}_s$.

ω_0 represents the resonant frequency of the system circuit. relay, and receiver are ω_1, ω_2, and ω_3, respectively. The relationship between these resonant frequencies and the compensation network parameters is as follows:

$$
\begin{cases}
\omega_1 = \dfrac{1}{\sqrt{(L_P - L_{P1})C_P}} \\[2mm]
\omega_2 = \dfrac{1}{\sqrt{L_1 C_1}} = \dfrac{1}{\sqrt{L_2 C_2}} \\[2mm]
\omega_3 = \dfrac{1}{\sqrt{L_S C_S}}
\end{cases}
\tag{1}
$$

Based on the relationship between the compensation network and the resonant frequency, the system's equivalent circuit can be further simplified as shown in Fig. 3 when $\omega_0 = \omega_1 = \omega_2 = \omega_3$.

Based on Figs 1 and 3, the system's quadratic characteristic equation is expressed as follows.

$$
\left(j\omega L + R + \frac{C}{j\omega} \right)
\begin{bmatrix} \dot{I}_1 \\ \dot{I}_2 \\ \dot{I}_3 \end{bmatrix}
= -j\omega
\begin{bmatrix} M_{P1} \\ M_{P2} \\ M_{P3} \end{bmatrix} \dot{I}_P
\tag{2}
$$

Here, the matrices L, R, and C are defined as follows:

$$
L =
\begin{bmatrix}
L_1 & M_{12} & M_{1S} \\
M_{12} & L_2 & M_{2S} \\
M_{1S} & M_{2S} & L_S
\end{bmatrix}
\tag{3}
$$

$$
R =
\begin{bmatrix}
R_1 & 0 & 0 \\
0 & R_2 & 0 \\
0 & 0 & R_{Leq}
\end{bmatrix}
\tag{4}
$$

$$
C =
\begin{bmatrix}
C_1^{-1} & 0 & 0 \\
0 & C_2^{-1} & 0 \\
0 & 0 & C_S^{-1}
\end{bmatrix}
\tag{5}
$$

In the figure, R_{Leq} is the equivalent load resistance of the rectifier output, which can be expressed as:
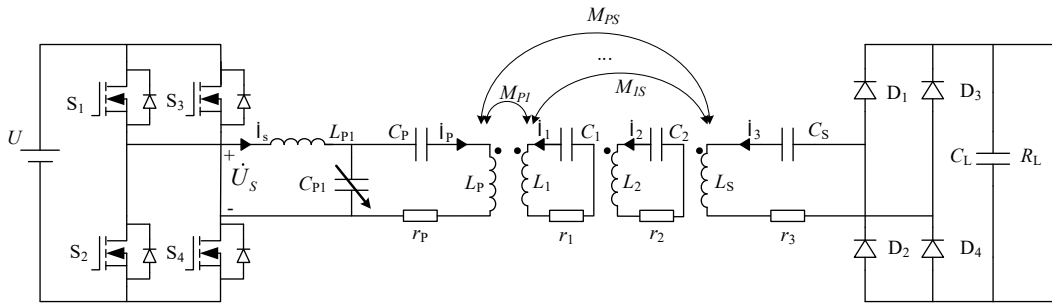
$$
R_{Leq} = \frac{8}{\pi^2} R_L
\tag{6}
$$

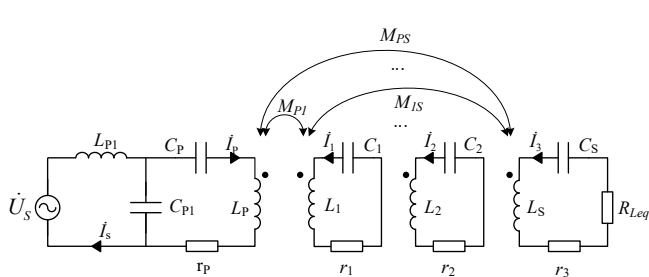**Fig. 1** Circuit topology of LCC-S multi-relay WPT system.

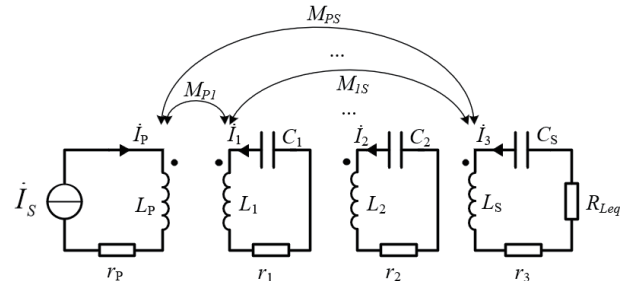**Fig. 2** Equivalent circuit diagram of LCC-S type multi-relay WPT system.

Fig. 3 Simplified equivalent circuit diagram of LCC-S type multi-relay WPT system.

At system resonance, $\frac{1}{j\omega C_1} + j\omega L_1 = \frac{1}{j\omega C_2} + j\omega L_2 = \frac{1}{j\omega C_S} + j\omega L_S = 0$ occurs, and the current relationship can be derived according to Kirchhoff's laws as:

$$\begin{bmatrix} \frac{1}{j\omega C_{P1}} + j\omega L_{P1} & \frac{1}{j\omega C_P} & 0 & 0 & 0 \\ \frac{1}{j\omega C_{P1}} & \frac{1}{j\omega C_{P1}} + \frac{1}{j\omega C_P} + j\omega L_P & j\omega M_{12} & j\omega M_{13} & j\omega M_{14} \\ 0 & j\omega M_{12} & 0 & j\omega M_{23} & j\omega M_{24} \\ 0 & j\omega M_{13} & j\omega M_{23} & 0 & j\omega M_{34} \\ 0 & j\omega M_{14} & j\omega M_{24} & j\omega M_{34} & R_L \end{bmatrix} \cdot$$

$$\begin{bmatrix} \dot{I}_S \\ \dot{I}_P \\ \dot{I}_1 \\ \dot{I}_2 \\ \dot{I}_3 \end{bmatrix} = \begin{bmatrix} \dot{U}_S \\ 0 \\ 0 \\ 0 \\ 0 \end{bmatrix}$$

(7)

From Eq. (7), the current in each branch/path of the system can be derived.

Additionally, by solving the KVL equation, the input and output active power, as well as the transmission efficiency of the system, can be determined. The specific formulas are as follows:

$$P_{\text{out}} = I_3{}^2 R_L \tag{8}$$

$$P_{\text{in}} = I_P{}^2 r_P + I_1{}^2 r_1 + I_2{}^2 r_2 + I_3{}^2 (R_3 + R_L) \tag{9}$$

$$\eta = \frac{P_{\text{in}}}{P_{\text{out}}} = \frac{R_L}{\left(\frac{I_P}{I_3}\right)^2 r_P + \left(\frac{I_1}{I_3}\right)^2 r_1 + \left(\frac{I_2}{I_3}\right)^2 r_2 + r_3 + R_L} \tag{10}$$

Due to the frequency-splitting phenomenon in this system, the system can maintain its highest output efficiency by adjusting the input frequency and the value of the resonant capacitor C_{P1} under different loads.

The LCC compensation network is used on the primary side of the system, and the current $\dot{I}_P$ is kept constant when the system operates at the constant-current resonant frequency. As shows in Eq. (11).

$$\dot{I}_P = -j\omega C_{P1} \dot{U}_S \tag{11}$$

Analysis of system output characteristics

Assuming the capacitance and resistance values of the coil remain constant, the constant-voltage and constant-current frequencies of this system can be determined through the Eq. (2) calculation. The corresponding compensation network parameters can then be derived based on these frequencies. Simulation platforms are utilized to obtain the output data of the aforementioned system under different operating frequencies and equivalent loads.

When the equivalent resistance R_{Leq} is 100, 200, 300, 400, and 500 Ω, the frequency-dependent curves of the output current I_{Out} and output voltage U_{Out} for the four-coil wireless power transfer system are shown in Figs 4 and 5, respectively.

As shown in Figs 4 and 5, this four-coil WPT system exhibits two constant current frequencies and three constant voltage frequencies, all marked in the figures. At these critical frequencies, the system ensures either constant voltage or constant-current output characteristics.

Based on the above equations[15], the specific values of the constant-current and constant-voltage operating frequencies for the four-coil WPT system can be calculated, as shown in Table 1. Here, CC1 and CC2 represent the first and second constant-current points, respectively, while CV1, CV2, and CV3 denote the first, second, and third constant voltage points, respectively.

After determining the system's key frequencies, MATLAB simulations were used to calculate the transmission efficiency at each
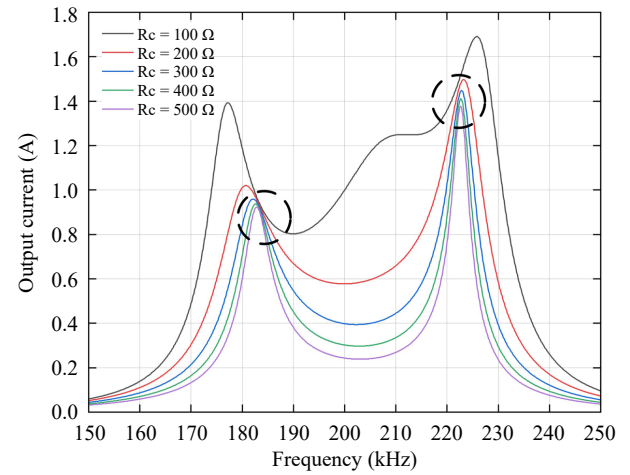

Fig. 4 Four-Coil WPT system output current versus frequency curve.
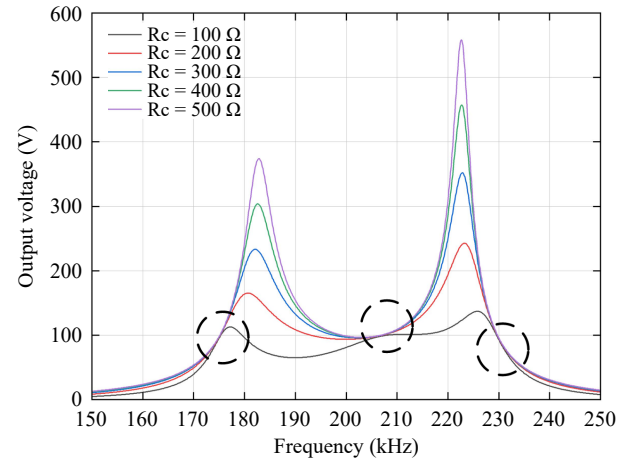

Fig. 5 Four-coil WPT system output voltage versus frequency curve.

frequency for different load resistances, providing results for the five key frequencies.

The simulation results in Fig. 6 demonstrate that the transmission efficiency varies across different key frequencies, peaking at 206 kHz. Therefore, the system can adjust the input frequency based on the output load and the requirements for constant current, constant voltage, and efficiency.

Figure 7 below shows the dot-line graphs of the five key frequencies at multiple resistances. These diagrams clearly illustrate the resistance values corresponding to the highest efficiency at each frequency.

The efficiency dot-line diagram shows that when the system load resistance ranges between 80 and 100 Ω, the transmission efficiency at the five key frequencies remains relatively high. Specifically, the efficiency reaches 86.67% at 206 kHz, while the efficiencies at the other four frequencies also exceed 75%.

In practical experiments, the phase difference between the inverter's output voltage and current varies with the load resistance,

Table 1. Four-Coil WPT system constant current and constant voltage frequency.

Current frequency	Operating frequency (KHz)	Voltage frequency	Operating frequency(KHz)
CC1	183	CV1	175
CC2	222	CV2	206
		CV3	225
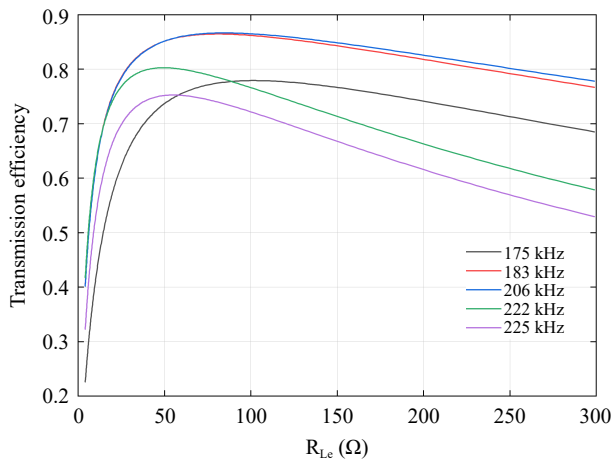
Fig. 6 System transmission efficiency at five critical frequencies.
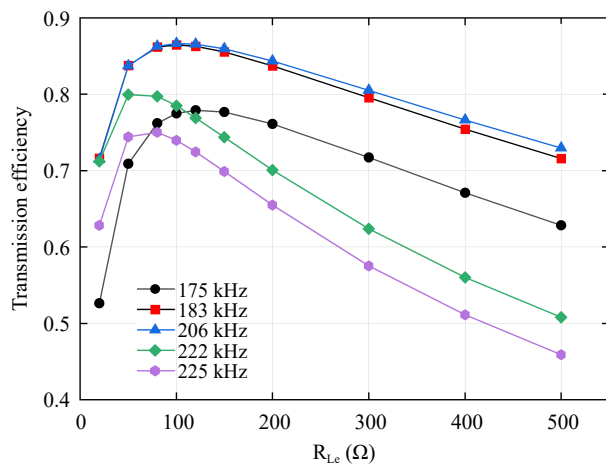
Fig. 7 Dot plot of efficiency at five key frequencies.

resulting in imprecise implementation of zero-voltage switching (ZVS) at the 183 kHz frequency. If the system does not operate under ZVS conditions, the power losses increase significantly. At 206 kHz, simulation results indicate that a constant-voltage output cannot be achieved. Therefore, neither of these two frequencies can be selected when a low-loss operation or constant-voltage output is required, and the choice must be made among the remaining three frequencies. This facilitates the selection of the most efficient frequency based on load variations, thereby demonstrating the necessity of employing a switched-capacitor matrix.

The switched capacitor matrix proposed in this paper demonstrates remarkable applicability in WPT systems due to its unique dynamic reconfigurability. This technical solution is compatible with multi-relay WPT systems of any topology and effectively addresses resonance point deviation caused by frequency splitting phenomena.

Study of resonant capacitance matrix

To address the impact of input frequency changes on the system's resonant state, this study designs a multi-capacitance matrix based on MOSFET switches. By combining capacitors of different values in series and parallel, this matrix flexibly adjusts the equivalent capacitance of the C_{P1} component, ensuring the system remains in resonance as the input frequency changes. Although transmission efficiency differs across frequencies, load resistors exhibit varying efficiencies at different frequencies. To better adapt

to these variations, the multi-capacitor matrix allows for convenient reconfiguration of capacitance after load adjustments, thereby optimizing system performance and ensuring optimal transmission results under diverse operating conditions.

Figure 8 illustrates the schematic diagram of the C_{P1} switched-capacitor matrix, where SW1, SW2, SW3, SW4, SW5, and SW6 are MOSFET switches, and C_{Z1}, C_{Z2}, and C_{Z3} are fixed-value capacitors. According to (1), the required resonant capacitance is calculated based on the obtained key frequencies. When the system's input frequency changes, the resonant capacitance value at the key frequency also changes. This study employs a switched-capacitor matrix method, where the equivalent capacitance is adjusted through the series-parallel combination of fixed capacitors in the matrix to match the resonant capacitance required by the current input frequency, ensuring high-efficiency transmission.

Through precise timing control, SCC ensures that no more than two parallel paths are conducted simultaneously during operation. This selective conduction mechanism significantly reduces the system's equivalent on-resistance while concentrating switching losses within a limited number of active branches. Furthermore, by optimizing the MOSFET driver circuit design and employing low-loss capacitors, additional losses are effectively mitigated, enabling the system to achieve high-efficiency power transfer.

The four operating modes of this switched-capacitor matrix are as follows:

Mode 1: When the upper MOSFET is turned on and the lower MOSFET is off, current can flow forward (from top to bottom) through the fixed capacitor, the upper MOSFET switch, and the diode connected to the lower switch, enabling the capacitor to function. However, if the current flows in an opposite direction, it is blocked and cannot operate.

Mode 2: When neither the upper nor the lower MOSFET is conducting, the system is in an open-circuit state.

Mode 3: When the lower MOSFET is turned on and the upper MOSFET is off, current can flow in reverse (from bottom to top) through the lower MOSFET switch, the diode connected to the upper switch, and the fixed capacitor, enabling the capacitor to function. However, if the current reverses again, it is blocked and cannot operate.

Mode 4: When both the upper and lower MOSFETs are turned on, the current can flow in both forward and reverse directions, allowing the system to operate normally.

Since this is an AC system, two reverse-series MOSFETs can control the current and prevent backflow, thereby protecting the entire system.

Figure 9 shows the four operating modes of a branch in the switched-capacitor matrix.
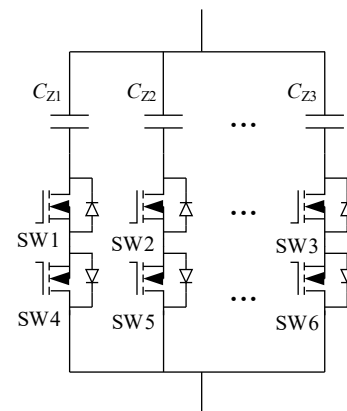
Fig. 8 Schematic diagram of switched capacitor matrix.

The switched-capacitor matrix imposes relatively low timing requirements because its channel switching operates non-real-time, controlling each path's on/off state through MOSFET switch regulation. Each MOSFET switch is connected to a dedicated driver circuit, with the STM32F407ZGT6 microcontroller providing PWM signals to
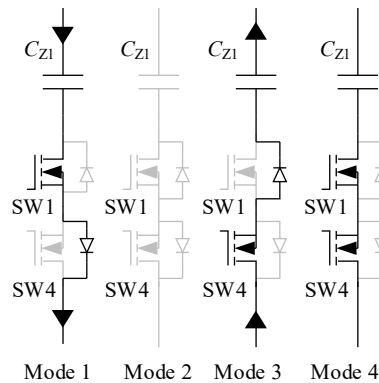
Fig. 9 Four operation modes of switched capacitor matrix.
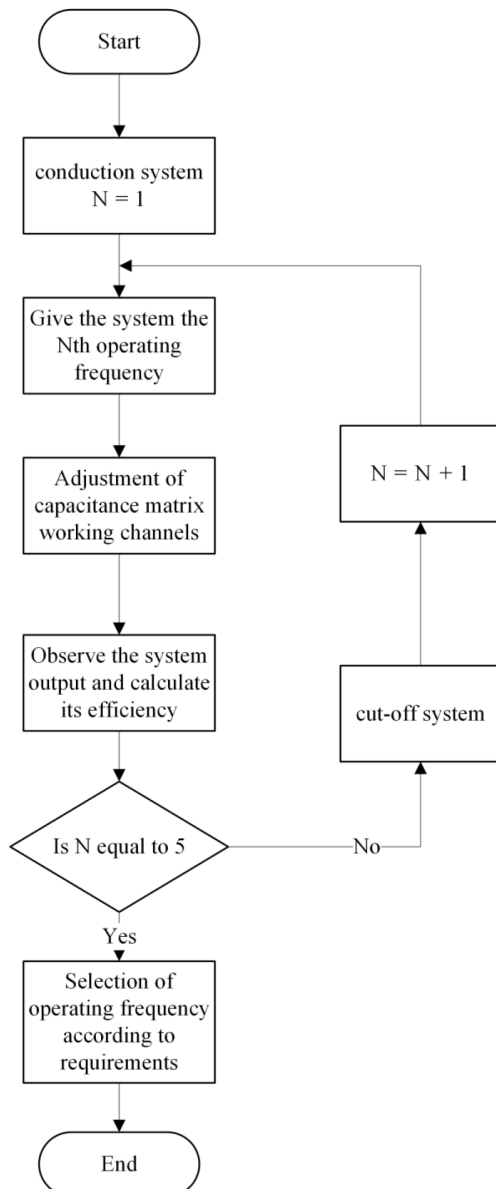
Fig. 10 System control block diagram.

these driver circuits for switch control. The STM32F407ZGT6 firmware implements a key-press interface to sequentially switch PWM output paths across predefined frequencies (starting at 175 kHz), cycling ascendingly to activate corresponding drivers. The selected MOSFET stays on until the next frequency change.

To simplify the experimental design, the current research phase focuses exclusively on validating the switched compensation capacitors topology and control methodology, deliberately excluding efficiency monitoring to avoid measurement-induced parameter interference. Subsequent studies will incorporate output-side monitoring equipment for complete efficiency characterization. The control block diagram is shown in Fig. 10.

Utilizing the series-parallel relationships of capacitors and combining capacitors with different capacitance values, the equivalent capacitance is adjusted to the value required for system resonance. When the input frequency is applied, a trigger signal is sent to the MOSFET switch connected in series with the resonant capacitor, which is turned on and ensures the system remains in resonance. This offline switching method enables faster and more precise identification of peak efficiency compared to real-time switching, which demonstrates inferior performance in maximum efficiency tracking.

Experimental verification

The capacitance values of each fixed-value capacitor in Fig. 8 are shown in Table 2, and the required resonant capacitance capacitance values at each critical frequency and the selection in the corresponding capacitance matrix are shown in Table 3.

The specific parameters of the components of the whole system during simulation are shown in Table 4.

Table 2. Values of the fixed capacitances in the capacitance matrix.

Capacitance number	Capacitance value (nF)
C_{Z1}	12
C_{Z2}	12
C_{Z3}	6.8
C_{Z4}	27
C_{Z5}	22
C_{Z6}	2.7

Table 3. Values of resonant capacitance at different key frequencies.

Frequency (KHz)	Selection of capacitance matrix
175	C_{Z4}
183	C_{Z1}, C_{Z2}
206	C_{Z5}
222	C_{Z1}, C_{Z3}
225	C_{Z1}, C_{Z6}

Table 4. Element parameters of four-coil multi-relay compensation network.

Parameters	Values
U (V)	100
L_P (μH)	30
L_{P1}, L_1, L_2, L_S (μH)	365
M_{P1}, M_{12}, M_{2S} (μH)	68
M_{P2}, M_{1S} (μH)	22
M_{PS} (μH)	10
C_P (nF)	1.9
C_1, C_2, C_S (nF)	1.73
C_L (μF)	2

In the simulation process, the value of C_{P1} is adjusted as the input frequency of the system is changed, so that the system remains in a resonant state. At this frequency, the transmission efficiency of the system reaches its highest level.

Figure 11 illustrates an experimental platform built based on the four-coil LCC-S multi-relay WPT system shown in Fig. 1. The input voltage was set to 40 V.

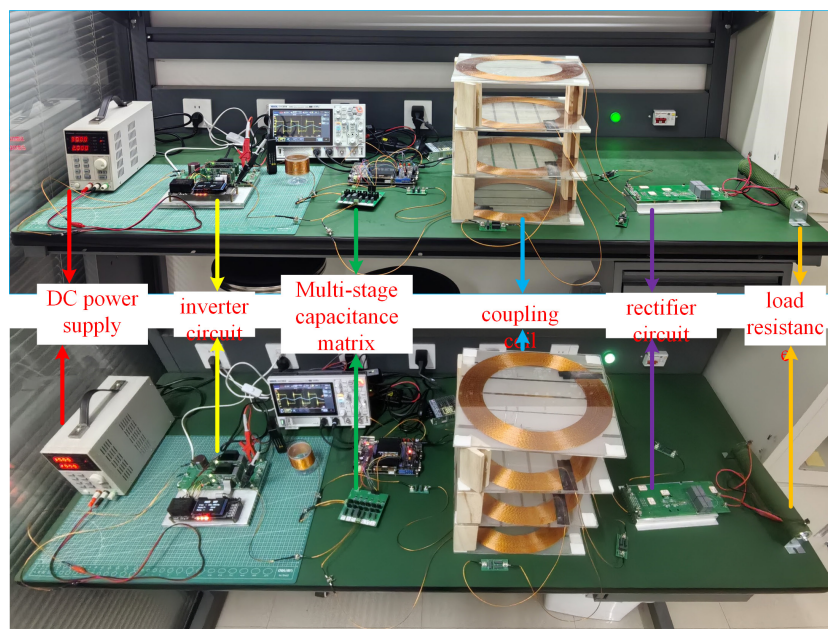The experimental waveforms confirm that the system can achieve

Fig. 11   LCC-S type multi-relay WPT system experimental device.

175KHz input waveform

183KHz input waveform

206KHz input waveform
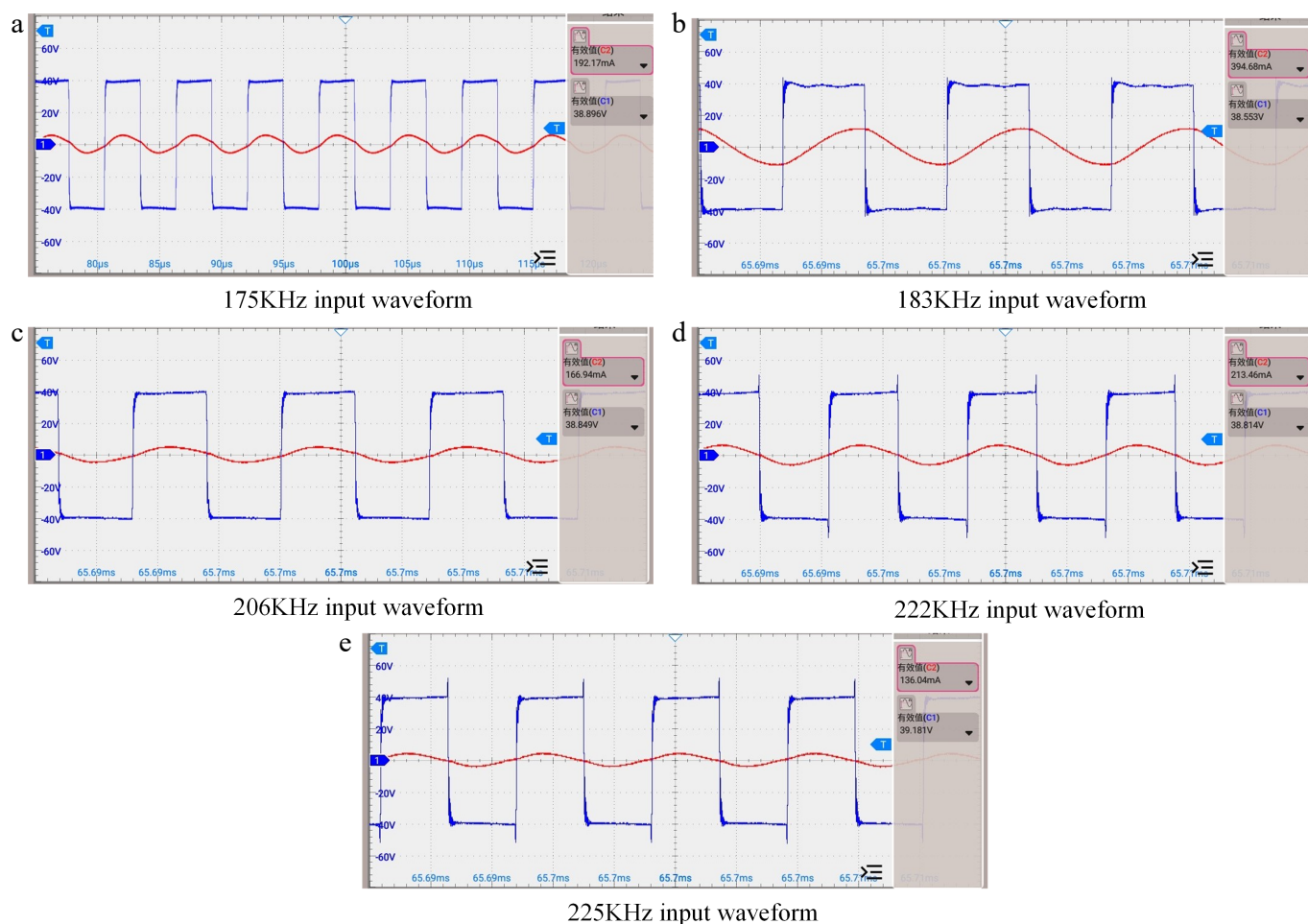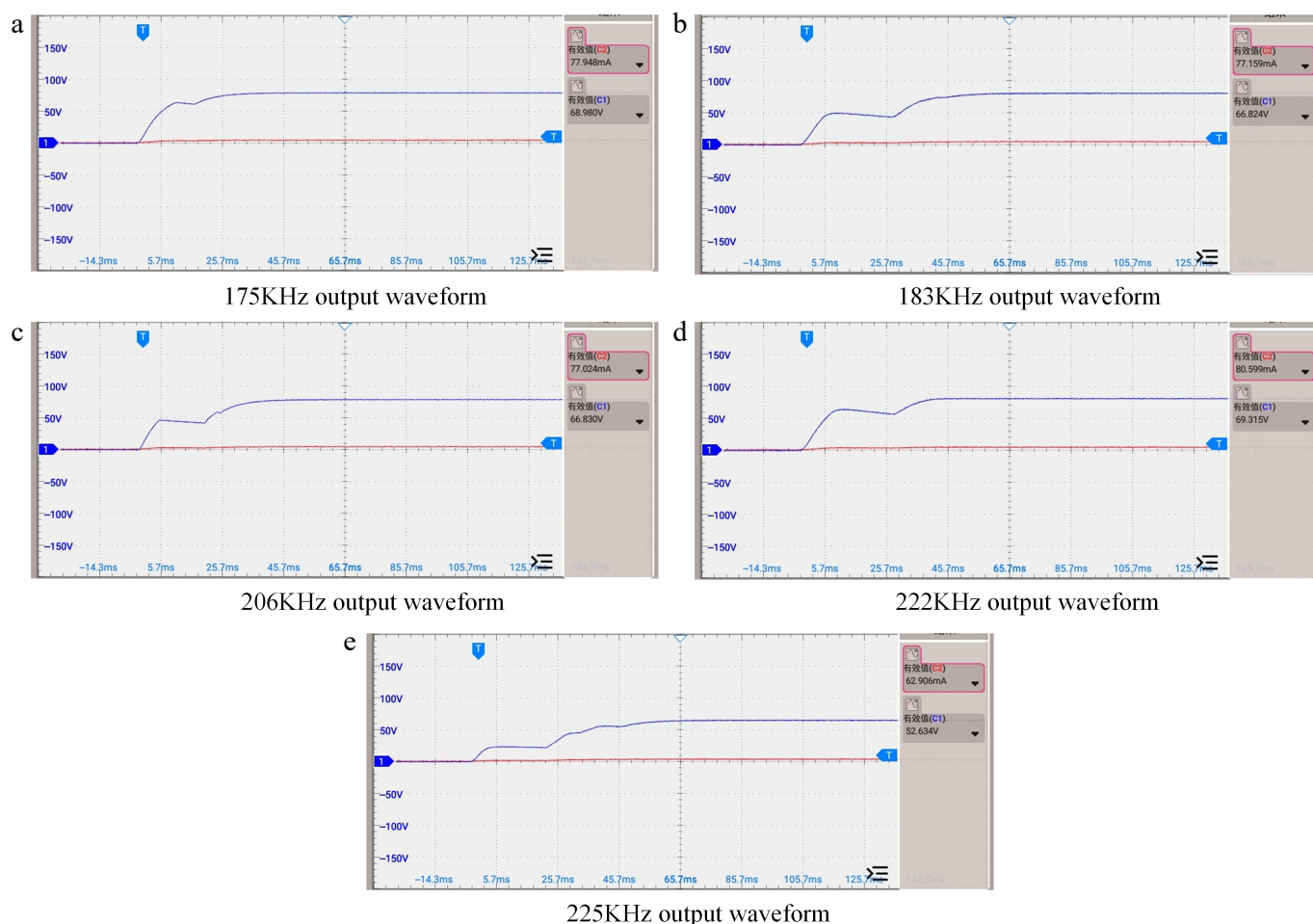
222KHz input waveform

225KHz input waveform

Fig. 12   Input waveform of experimental equipment.

Fig. 13 Output waveform of experimental equipment.

Table 5. Experimental transmission power and efficiency of four-coil WPT system at different input frequencies.

Frequency (KHz)	Equivalent load (Ω)	Transmission efficiency
175	100	71.94%
183	100	42.07%
206	100	79.37%
222	100	71.94%
225	100	62.11%

ZVS (zero-voltage switching) and constant current/voltage output at key frequencies. Figure 12 shows the input waveform of the compensation network. Figure 13 shows the system's output waveforms at these five key frequencies.

Based on the comparison of simulation and experimental data, the system's simulated efficiency is higher than the experimental results because the simulation does not account for losses from measuring instruments.

Table 5 presents the transmission efficiency results from the hardware experiments.

Conclusions

In this paper, a mathematical model of a four-coil wireless power transfer (WPT) system is established based on circuit theory, and the system's output characteristics are thoroughly analyzed to determine its constant voltage and constant current frequencies. However, in the four-coil LCC-S compensation network WPT system, changes in the input frequency can lead to resonant capacitance mismatch, significantly reducing transmission efficiency. An innovative solution is proposed to address this issue: a capacitance matrix method is introduced to optimize the compensation capacitance of the four-coil WPT system.

Finally, an experimental platform for this system was constructed, and the resonant capacitor C_{P1} in the four-coil WPT system was improved. The experimental results demonstrate that the enhanced C_{P1} can more conveniently match the corresponding resonant capacitor as the input frequency changes. This effectively ensures the system's transmission efficiency and verifies the feasibility and effectiveness of the proposed method.

Author contributions

The authors confirm their contributions to the paper as follows: study conception and design: Hou X, Yang M, Shi Y, Yu Z, Zhao Z; data collection: Yang M; analysis and interpretation of results, draft manuscript preparation: Hou X, Yang M. All authors reviewed the results and approved the final version of the manuscript.

Data availability

All data analyzed during this study are available from the corresponding author upon reasonable request.

Acknowledgments

Conflict of interest

The authors declare that they have no conflict of interest.

Dates

References

1. Zhang Z, Zhang B, Deng B, Wei X, Wang J. 2018. Opportunities and challenges of metamaterial-based wireless power transfer for electric vehicles. *Wireless Power Transfer* 5(1):9−19
2. Su Y, Zhou W, Hu A, Sun Y, Chen L. 2015. A power-signal parallel transmission technology for ECPT systems based on duty cycle modulation of square wave carrier. *Transactions of China Electrotechnical Society* 30(21):51−56
3. Guo Z, Nai J, Chen S, Zhang H, Ye M, et al. 2025. Optimized configuration and characterization of LCC-S based wireless power transmission system. *Wireless Power Transfer* 12:e012
4. Hu J, Luo C, Hong Y, Wang G, Fan X, et al. 2025. Deployment optimization of laser chargers in self-organizing power transfer internet of things. *Wireless Power Transfer* 12:e010
5. Li Y, Gui L, Jiang Y, Jing R, Li Y, et al. 2024. Optimal configuration of single-layer domino-coils with uniform spacing for online monitoring equipment in smart grid. *IEEE Transactions On Power Electronics* 39(11):14307−17
6. Wu Z, Tan L, Xu H, Shen S, Huang X. 2024. Design of the long-distance wireless power transfer system with multiple relay coils based on loss optimization. *Electrical Engineering* 106(3):3337−48
7. Li X, Yin W, Zhou X, Wang C, Sun W, et al. 2024. Analysis of wireless power transfer characteristics with multiple relay coils based on COMSOL. *Journal of Mudanjiang Normal University (Natural Sciences Edition)* 2024(2):31−35 (in Chinese)
8. Gu WJ, Harada K. 1988. A new method to regulate resonant converters. *IEEE Transactions on Power Electronics* 4(3):430−39
9. Wang X Q, Xu J P, Leng M R, Ma, He S Z. 2021. A hybrid control strategy of LCC-S compensated WPT system for wide output voltage and ZVS range with minimized reactive current. *IEEE Transactions on Industrial Electronics* 68(9):7908−20
10. Pang H, Xu F, Liu W, Tse Chi K, Chau KT. 2024. Impedance Buffer-based reactance cancellation method for CLC-S compensated wireless power transfer. *IEEE Transactions on Industrial Electronics* 71(7):6894−906
11. Cao L, Bao J, Loo KH, Pan X, Zhang R. 2023. A hybrid control strategy for dynamic compensation of cross-coupling effect in two-load IPT system. *IET Power Electronics* 16(12):1943−57
12. Chen C, Zhou H, Deng Q, Hu W, Yu Y, et al. 2019. Modeling and design of zero-voltage-switching controller for wireless power transfer systems based on closed-loop dominant pole. *Journal of Power Electronics* 19(5):1235−47
13. Yu Z, Shan M, Du H, Lei Y. 2024. Global optimization of transmission efficiency in multi-relay MC-WPT system based on switching topology for enhanced tracing. *IEEE 2nd International Conference on Power Science and Technology (ICPST), 9−11 May 2024, Dali, China*. pp. 763−68 doi: 10.1109/ICPST61417.2024.10602044
14. Hou X, Xia H, Shi Y. 2023. Research on segmented compensation technology for three-coil WPT system. *Journal of Power Supply* 21(6):49−56
15. Hou X, Su Y, Zuo Z, Dai X, Fei Y. 2021. A novel analysis method based on quadratic eigenvalue problem for multirelay magnetic coupling wireless power transfer. *IEEE Transactions on Power Electronics* 36(9):9907−17